Microstructure-dependent dynamic behavior of torsional nano-varactor

Article *in* Measurement · July 2017

DOI: 10.1016/j.measurement.2017.07.011

4 authors, including:

Hamid M Sedighi
Shahid Chamran University of Ahvaz
78 PUBLICATIONS **627** CITATIONS
SEE PROFILE

Mohamadreza Abadyan
Shahrekord Branch, Islamic Azad University
93 PUBLICATIONS **1,193** CITATIONS
SEE PROFILE

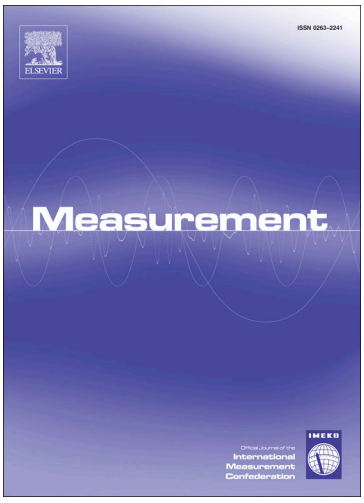

Microstructure-dependent dynamic behaviour of torsional nano-varactor

Hamid Mohamad-Sedighi, Ali Koochi, Maryam Keivani, Mohamadreza Abadyan

PII: S0263-2241(17)30446-3
DOI: http://dx.doi.org/10.1016/j.measurement.2017.07.011
Reference: MEASUR 4851

To appear in: *Measurement*

Received Date: 28 November 2015
Revised Date: 19 January 2017
Accepted Date: 10 July 2017

Please cite this article as: H. Mohamad-Sedighi, A. Koochi, M. Keivani, M. Abadyan, Microstructure-dependent dynamic behaviour of torsional nano-varactor, *Measurement* (2017), doi: http://dx.doi.org/10.1016/j.measurement.2017.07.011

Microstructure-dependent dynamic behaviour of torsional nano-varactor

Hamid Mohamad-Sedighi[1], Ali Koochi[2,*], Maryam Keivani[3], Mohamadreza Abadyan[2]

[1]*Mechanical Engineering Department, Faculty of Engineering, Shahid Chamran University of Ahvaz, Ahvaz 61357-43337, Iran*
[2] *Shahrekord Branch, Islamic Azad University, Shahrekord, Iran*
[3] *Shahrekord University of Medical Sciences, Shahrekord, Iran*

Abstract

Experiments depict that the physico-mechanical response of miniature devices is microstructure-dependent. However, the classic continuum theory cannot correctly predict the microstructure-dependency. In this paper, the strain gradient theory is employed to examine the dynamic behavior and instability characteristics of miniature varactor with trapezoidal geometry. The governing equation of the varactor is obtained incorporating the effects of Coulomb force, van der Waals (vdW) attraction, squeeze film damping and structural damping. The influences of microstructure on the dynamic instability of equilibrium points are studied by plotting the phase portrait and bifurcation diagrams. It is found that increase in the microstructure parameter enhances the torsional stability. In the presence of the applied voltage, the phase portrait shows the saddle-node bifurcation while for free-standing varactor a subcritical pitchfork bifurcation is observed.

Keywords: nano-electromechanical varactor; microstructure; strain gradient theory; dynamic instability; van der Waals force.

1. Introduction

Ultra-small electrostatic torsional actuators due to the high sensitivity, high quality factor, low actuation voltage and small possibility of stiction have wide applications in the micro/nano-electromechanical systems (MEMS/NEMS) such as tunable torsional capacitors, digital light processing chips and torsional radio frequency switches used in micro-satellite communications and radar systems [1-5]. Among these systems, torsional NEMS varactors are being considered as potential ultra-small devices with promising applications in fabrication of smart structures such as confocal microscopy, wireless communications, optical telecommunication, bar code reading, laser printing and endoscopic bio-imaging, integrated circuits, switching devices, nano-robots, etc. Therefore, many researchers have focused on the numerical, theoretical and experimental analysis of such systems through different assumptions and methods [6-14]. The torsional nano-varactor is composed of movable conductive electrode (mainplate) which is suspended over a fixed conductive electrode (substrate) using torsional nano-beams. In the equilibrium position, the electrostatic and restoring forces/torques are identical. However, if the potential difference exceeds its critical value, the nano-varactor becomes structurally instable and the flexible plate adheres to the fixed substrate i.e. pull-in instability occurs. Actually, pull-in is an unstable state at which the elastic torque can no more balance the electrical torque [15, 16]. The pull-in instability phenomenon is a crucial issue in the design and fabrication of NEMS/MEMS. Recently, many investigations have extensively focused on the prediction of pull-in state of electrostatic torsional NEMS/MEMS [17-22]. Sedighi and Shirazi [18] investigated the nonlinear behavior of double-sided-actuated torsional nano-switches with different actuation voltages. Guo et al. [19] studied the pull-in instabilities of a rotational MEMS/NEMS in the presence of capillary effects. The chaotic behavior in torsional MEMS mirrors near the instability condition was developed by Shabani et al. [20].

* *Corresponding author email:abadyan@yahoo.com*

If the dimensions of structures reduce to the sub-micron scale, the electromechanical response of such devices might be microstructure-dependent. The microstructure-dependency is an intrinsic property of some materials when the characteristic size of the nanostructures is comparable with the material length scale [23]. From this point of view, new parameters which can predict the microstructure effects should be included in the theoretical governing equations. Unfortunately, the classical continuum mechanics is not able to explain the microstructure-dependent behaviors of miniature structures. Instead, new non-classical models such as modified couple stress theory [24] and strain gradient theory (SGT) [25] - which incorporates the microstructure effects in the governing equation - can be employed. Lam et al. [25], developed a modified SGT with three material length scale parameters. In this work the authors employ SGT for modeling the microstructure-dependent dynamic and instability of the nano-varactor.

To the best knowledge of authors, the effect of microstructure on the dynamic characteristics of torsional NEMS varactors has not been addressed till present. The main goal of the present article is to investigate the influence of microstructure phenomenon on the dynamic response and instability threshold of trapezoidal NEMS varactor operating in vdW regime. The presence of vdW force significantly affects the behavior of ultra-small structures. Although the vdW force can be ignored in designing micro-scale actuators, it plays crucial role at submicron [26-31]. The equation of motion is extracted based on the strain gradient elasticity and with the consideration of structural damping. To examine the stability of the equilibrium points of the nano-system, bifurcation diagrams and phase portraits are plotted and discussed.

2. Mathematical formulation

Figure 1 shows the schematic configuration and side views of a torsional NEMS varactor. The mainplate is suspended over the ground electrode via two elastic nano-scale beams with length L. The initial gap between mainplate and fixed substrate is g and the rotation of mainplate is denoted by θ.

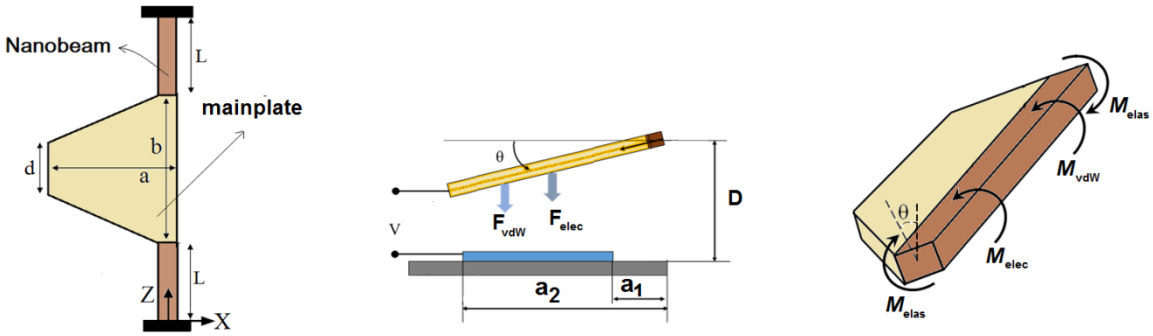

Fig. 1 Schematics of a torsional nano-varactor

2.1 Basic idea of SGT

Based on the SGT, the strain energy density, $\bar{U}$, can be explained as [25]:

$$\bar{U} = \frac{1}{2}\left(\sigma_{ij}\,\varepsilon_{ij} + p_i\,\gamma_i + \tau^{(1)}_{ijk}\,\eta^{(1)}_{ijk} + m^{s}_{ij}\,\chi^{s}_{ij}\right), \tag{1}$$

in which

$$\varepsilon_{ij} = \frac{1}{2}\left(u_{i,j} + u_{j,i}\right) \tag{2}$$

$$\gamma_i = \varepsilon_{mm,i} \tag{3}$$

$$\eta_{ijk}^{(1)} = \frac{1}{3}\left(\varepsilon_{jk,i} + \varepsilon_{ki,j} + \varepsilon_{ij,k}\right) - \frac{1}{15}\delta_{ij}\left(\varepsilon_{mm,k} + 2\varepsilon_{mk,m}\right) - \frac{1}{15}\left[\delta_{jk}\left(\varepsilon_{mm,i} + 2\varepsilon_{mi,m}\right) + \delta_{ki}\left(\varepsilon_{mm,j} + 2\varepsilon_{mj,m}\right)\right] \tag{4}$$

$$\chi_{ij}^{s} = \frac{1}{2}e_{jkl}u_{l,ki} \tag{5}$$

In above equations, u_i, γ_i, $\eta_{ijk}^{(1)}$, χ_{ij}^{s}, δ_{ij} and e_{ijk} are components of displacement vector, dilatation gradient vector, stretch gradient tensor, rotation gradient tensor, Kronocker delta and permutation symbol, respectively. Also σ_{ij}, p_i, $\tau_{ijk}^{(1)}$, m_{ij}^{s}, are respectively the components of Cauchy's stress and high order stress tensors that are determined as the following [25]:

$$\sigma_{ij} = 2\mu\left(\varepsilon_{ij} + \frac{\nu}{1-2\nu}\varepsilon_{mm}\delta_{ij}\right) \tag{6}$$

$$p_i = 2\mu l_0^2 \gamma_i \tag{7}$$

$$\tau_{ijk}^{(1)} = 2\mu l_1^2 \eta_{ijk}^{(1)} \tag{8}$$

$$m_{ij}^{s} = 2\mu l_2^2 \chi_{ij}^{s} \tag{9}$$

In the above equations, υ and μ are Poisson's ratio and shear modulus, respectively. Also l_0, l_1 and $l_2$are additional material length scale parameters to incorporate the microstructure dependency.

2.2 Governing equation

Using Newton's second law, the rotational motion of the mainplate is expressed by the following second order differential equation:

$$I_v\ddot{\theta} + (c_{st} + C_{SFD})\dot{\theta} + 2M_{elas} - M_{elect} - M_{vdW} = 0 \tag{10}$$

where I_v is the moments of inertia for the mirror, c_{st} is the structural damping coefficient and C_{SFD} is the squeeze film damping. In above relation, M_{elas}, M_{elect} and M_{vdW} are respectively elastic, electrical and vdW moments. The moment terms are calculated in the following subsections:

2.2.1. Elastic Moment

To determine the elastic moment, the displacement vector **u** of torsional beam and based on the Saint-Venant's formulation is assumed as:

$$\mathbf{u} = -\Omega z y e_1 + \Omega z x e_2 + \Omega\psi(x,y)e_3 \tag{11}$$

Where $\psi(x,y)$ is the warping function and Ω is angle of twist per unit length along the torsion beam. Furthermore, x and y are the coordinates of each point of cross section. Based on [32, 33], the elastic moment acts on a rectangular cross-section is written as

$$M_{elas} = \mu\Omega\int_A\left(x^2 + y^2 + x\frac{\partial\psi}{\partial y} - y\frac{\partial\psi}{\partial x}\right)dA + 3Al_2^2\mu\Omega = \mu\frac{\theta}{L}\left[\int_A\left(x^2+y^2\right)dA + \int_A\left(x\frac{\partial\psi}{\partial y} - y\frac{\partial\psi}{\partial x}\right)dA + 3Al_2^2\right] = \mu\frac{\theta}{L}\left(J + J_C\right) \tag{12}$$

where J is the polar moment of inertia for the torsional beam and J_c represent the microstructure-dependency of the elastic moment which is a function of material length scale parameters and for rectangular cross section can be expressed as:

$$J_c = 3Al_2^2 + \iint_A \left(x\frac{\partial \psi}{\partial y} - y\frac{\partial \psi}{\partial x} \right) dA \tag{13}$$

The warping function (ψ) can be numerically obtained (see the Appendix).

2.2.2 Electrostatic moment

The electrostatic force operating on an infinitesimal element of nano-varactor is written as [34]:

$$dF_{elec} = \frac{\varepsilon V^2}{2\left(g\text{-}X\ sin(\theta)\right)^2}\left[b - \left(\frac{b-d}{a}\right)X \right] dX \tag{14}$$

where V is the applied voltage. Based on the defined parameters in Fig. 1, the electrostatic force acts on this element of mainplate can be obtained as:

$$dM_{elec} = X\ cos(\theta) dF_{elec} = \frac{\varepsilon V^2}{2\left(g\text{-}Xsi\ n(\theta)\right)^2}\left[b - \left(\frac{b-d}{a}\right)X \right] X\ cos(\theta) dX \tag{15}$$

Finally by integrating equation (15), the electrical moment is given by:

$$M_{elec} = \int_{a_1}^{a_2} \frac{\varepsilon V^2}{2\left(g\text{-}Xsi\ n(\theta)\right)^2}\left[b - \left(\frac{b-d}{a}\right)X \right] X\ cos(\theta) dX \tag{16}$$

After some mathematical calculations, the electrical moment induced on the mainplate is simplified as:

$$\begin{aligned} M_{elec} = {} & \frac{\varepsilon V^2 b\, cos(\theta)}{2\sin^2\theta}\Bigg\{ \frac{g}{g - a_2 \sin\theta} - \frac{g}{g - a_1 \sin\theta} + ln\left(\frac{g - a_2 \sin\theta}{g - a_1 \sin\theta}\right) \\ & - \frac{(b\text{-}d)}{ab\sin\theta}\left[\frac{g^2}{g - a_2 \sin\theta} - \frac{g^2}{g - a_1 \sin\theta} + (a_2 - a_1)\sin\theta + 2g\ ln\left(\frac{g - a_2 \sin\theta}{g - a_1 \sin\theta}\right) \right] \Bigg\} \end{aligned} \tag{17}$$

for the case of small angle one can assume that $sin(\theta) \cong \theta, cos(\theta) \cong 1$, consequently we have:

$$\begin{aligned} M_{elec} = {} & \frac{\varepsilon V^2 b}{2\theta^2}\Bigg\{ \frac{g}{g - a_2\theta} - \frac{g}{g - a_1\theta} + ln\left(\frac{g - a_2\theta}{g - a_1\theta}\right) \\ & - \frac{(b\text{-}d)}{ab\theta}\left[\frac{g^2}{g - a_2\theta} - \frac{g^2}{g - a_1\theta} + (a_2 - a_1)\theta + 2g\ ln\left(\frac{g - a_2\theta}{g - a_1\theta}\right) \right] \Bigg\} \end{aligned} \tag{18}$$

2.2.3 van der Waals moment

The vdW force operating on an infinitesimal element of nano-varactor can be written as [35]:

$$dF_{vdW} = \frac{A}{6\pi\left(g\text{-}X\ sin(\theta)\right)^3}\left[b - \left(\frac{b-d}{a}\right)X \right] dX \tag{19}$$

where $\bar{A}$ is Hamaker constant. Thereby, the relations for the differential vdW moment applied on the infinitesimal element of mainplate is given by:

$$dM_{vdW} = \frac{A}{6\pi\left(g\text{-}Xsi\ n(\theta)\right)^3}\left[b - \left(\frac{b-d}{a}\right)X \right] X\ cos(\theta) dX \tag{20}$$

After some mathematical calculations, the vdW moment induced on the finite conductive mainplate is simplified as:

$$M_{vdW}=\int_0^a \frac{A}{6\pi\left(g\text{-}X\sin(\theta)\right)^3}\left[b-\left(\frac{b-d}{a}\right)X\right]X\cos(\theta)dX=$$

$$\frac{Ab\cos(\theta)}{12\pi g(g-a\sin\theta)^2\sin^3\theta}\{a^2\sin^3\theta+\frac{(b\text{-}d)g\sin\theta}{b}(2g-3a\sin\theta)+ \quad (21)$$

$$2\frac{g(b\text{-}d)}{ab}(g-a\sin\theta)^2\ln\left(\frac{g-a\sin\theta}{g}\right)\}$$

and for the case of small angle one can conclude that:

$$M_{vdW}=\frac{Ab}{12\pi g(g-a\theta)^2\theta^3}\{a^2\theta^3+\frac{(b\text{-}d)g\theta}{b}(2g-3a\theta) \quad (22)$$

$$+2\frac{g(b\text{-}d)}{ab}(g-a\theta)^2\ln\left(\frac{g-a\theta}{g}\right)\}$$

2.2.4 Squeeze film damping:

In this section a nonlinear formulation for the air damping for circular-type nano-varactor are presented. According to the Reynolds equation, the squeeze film damping force applied on the infinitesimal element of mainplate can be written as [36]:

$$\frac{dF_{SFD}}{\dot{v}}=-\frac{c_d}{\left(g\text{-}X\sin(\theta)\right)^3}\left[b-\left(\frac{b-d}{a}\right)X\right]dX \quad (23)$$

the moment of damping forces on each element can be explained as:

$$\frac{dM_{SFD}}{\dot{\theta}}=-\frac{c_d}{\left(g\text{-}X\sin(\theta)\right)^3}\left[b-\left(\frac{b-d}{a}\right)X\right]X\cos(\theta)dX \quad (24)$$

By integrating the above-mentioned relation we have:

$$C_{SFD}=-\iint_S\frac{dM_{SFD}}{\dot{\theta}}dS=\int_0^a\frac{c_d}{\dot{\theta}\left(g\text{-}X\sin(\theta)\right)^3}\left[b-\left(\frac{b-d}{a}\right)X\right]X\cos(\theta)dX \quad (25)$$

and finally the damping parameter are calculated as:

$$C_{SFD}=-\frac{c_d b\cos(\theta)\left\{a^2\sin^3\theta+\frac{(b\text{-}d)g\sin\theta}{b}(2g-3a\sin\theta)+2\frac{g(b\text{-}d)}{ab}(g-a\sin\theta)^2\ln\left(\frac{g-a\sin\theta}{g}\right)\right\}}{2g(g-a\sin\theta)^2\sin^3\theta} \quad (26)$$

for the case of small angle the non-linear damping coefficient can be simplified as:

$$C_{SFD}=\frac{c_d b}{2g(g-a\theta)^2\theta^3}\left\{a^2\theta^3+\frac{(b\text{-}d)g\theta}{b}(2g-3a\theta)+2\frac{g(b\text{-}d)}{ab}(g-a\theta)^2\ln\left(\frac{g-a\theta}{g}\right)\right\} \quad (27)$$

2.3 Dimensionless governing equation

By substituting equations (11), (17), (22) and (27) in Eq. (10) the equation of motion for trapezoidal nano-varactor including structural damping, microstructure effects and vdW force can be derived as:

$$I_v\ddot{\theta}+\left(c_{st}+\frac{c_d b}{2g(g-a\theta)^2\theta^3}\left\{a^2\theta^3+\frac{(b\text{-}d)g\theta}{b}(2g-3a\theta)+2\frac{g(b\text{-}d)}{ab}(g-a\theta)^2\ln\left(\frac{g-a\theta}{g}\right)\right\}\right)\dot{\theta}$$
$$+2\frac{\mu(J+J_C)}{L}\theta=$$
$$\frac{\varepsilon V^2 b}{2\theta^2}\left\{\frac{g}{g-a_2\theta}-\frac{g}{g-a_1\theta}+\ln\left(\frac{g-a_2\theta}{g-a_1\theta}\right)\right.$$
$$\left.-\frac{(b\text{-}d)}{ab\theta}\left[\frac{g^2}{g-a_2\theta}-\frac{g^2}{g-a_1\theta}+(a_2-a_1)\theta+2g\ln\left(\frac{g-a_2\theta}{g-a_1\theta}\right)\right]\right\} \tag{28}$$
$$+\frac{Ab}{12\pi g(g-a\theta)^2\theta^3}\left\{a^2\theta^3+\frac{(b\text{-}d)g\theta}{b}(2g-3a\theta)+2\frac{g(b\text{-}d)}{ab}(g-a\theta)^2\ln\left(\frac{g-a\theta}{g}\right)\right\}$$

Thereby, after some mathematical computations, the governing equation for the considered system can be summarized as:

$$\ddot{\Theta}+\left(\bar{C}+\frac{C_{nl}}{(1-\Theta)^2}\left\{1+\frac{1\text{-}\gamma}{\Theta^2}(2-3\Theta)+\frac{2\text{-}2\gamma}{\Theta^3}(1-\Theta)^2\ln(1-\Theta)\right\}\right)\dot{\Theta}$$
$$+\left(1+\frac{J_C}{J}\right)\Theta=\frac{\lambda^2}{\Theta^2}\left\{\frac{1}{1-\beta\Theta}-\frac{1}{1-\alpha\Theta}+\ln\left(\frac{1-\beta\Theta}{1-\alpha\Theta}\right)\right.$$
$$\left.-\frac{1\text{-}\gamma}{\Theta}\left[\frac{1}{1-\beta\Theta}-\frac{1}{1-\alpha\Theta}+(\beta-\alpha)\Theta+2\ln\left(\frac{1-\beta\Theta}{1-\alpha\Theta}\right)\right]\right\} \tag{29}$$
$$+\frac{\eta}{(1-\Theta)^2}\left\{1+\frac{1\text{-}\gamma}{\Theta^2}(2-3\Theta)+\frac{2\text{-}2\gamma}{\Theta^3}(1-\Theta)^2\ln(1-\Theta)\right\}$$

The nondimensional variables appearing in the governing equation (29) are defined as:

$$\gamma=\frac{d}{b},\alpha=\frac{a_1}{a},\beta=\frac{a_2}{a},\theta_{max}=\frac{g}{a},\ \Theta=\frac{\theta}{\theta_{max}},\tau=\sqrt{\frac{2\mu J}{LI_v}}t,$$
$$\eta=\frac{Ab\,a^2}{12\pi g^3}\quad\lambda=V\sqrt{\frac{\varepsilon L}{4\theta_{max}^2\mu J}},\ \bar{C}=c_{st}\sqrt{\frac{L}{2\mu JI_v}},\ C_{nl}=\frac{c_d b\,a^2}{2g^3}\sqrt{\frac{L}{2\mu JI}}, \tag{30}$$

2.4. Dynamic stability analysis

To examine the dynamic stability of nano-varactor, the governing equation described in (30) is considered. To this end, the differential equation should be defined using the state space variables as:

$$\begin{bmatrix}q_1\\q_2\end{bmatrix}=\begin{bmatrix}\Theta\\\dot{\Theta}\end{bmatrix} \tag{31}$$

where q_1 and q_2 are the state space variables. In addition, by considering this kind of formulations, the bifurcation diagrams and phase portraits of the system can be plotted and the stability of fixed points are also investigated. Therefore, the governing equation (30) reduces to the following first-order differential equation:

$$\begin{bmatrix}\dot{q}_1\\\dot{q}_2\end{bmatrix}=\begin{bmatrix}F_1(q_1,q_2)\\F_2(q_1,q_2)\end{bmatrix} \tag{32}$$

where

$$F_1(q_1,q_2)=q_2 \tag{33}$$

$$F_2(q_1,q_2) = -(\bar{C} + \frac{C_{nl}}{(1-q_1)^2}\left\{1 + \frac{1-\gamma}{{q_1}^2}(2-3q_1) + \frac{2-2\gamma}{{q_1}^3}(1-q_1)^2 \ln(1-q_1)\right\})q_2$$
$$-(1+\frac{J_c}{J})q_1 + \frac{\lambda^2}{{q_1}^2}\{\frac{1}{1-\beta q_1} - \frac{1}{1-\alpha q_1} + \ln\left(\frac{1-\beta q_1}{1-\alpha q_1}\right)$$
$$-\frac{1-\gamma}{q_1}\left[\frac{1}{1-\beta q_1} - \frac{1}{1-\alpha q_1} + (\beta-\alpha)q_1 + 2\ln\left(\frac{1-\beta q_1}{1-\alpha q_1}\right)\right]\} \quad (34)$$
$$+\frac{\eta}{(1-q_1)^2}\left\{1 + \frac{1-\gamma}{{q_1}^2}(2-3q_1) + \frac{2-2\gamma}{{q_1}^3}(1-q_1)^2 \ln(1-q_1)\right\}$$

It should be noted that the positions of equilibrium points are determined by setting the right-hand side of equation (33) and (34) equal to zero. On the other hand, to examine the local stability in the vicinity of each fixed point, the Jacobian matrix is defined as follows:

$$Jacobian = \begin{bmatrix} \frac{\partial F_1(q_1,q_2)}{\partial q_1} & \frac{\partial F_1(q_1,q_2)}{\partial q_2} \\ \frac{\partial F_2(q_1,q_2)}{\partial q_1} & \frac{\partial F_2(q_1,q_2)}{\partial q_2} \end{bmatrix} = \begin{bmatrix} 0 & 1 \\ \frac{\partial F_2(q_1,q_2)}{\partial q_1} & \frac{\partial F_2(q_1,q_2)}{\partial q_2} \end{bmatrix} \quad (35)$$

By computing the eigenvalues (λ) of the Jacobian matrix, the stability of the equilibrium points of the system can be checked [37, 38]. The solution of the characteristic equation for Jacobian matrix is simplified to:

$$\lambda_{1,2} = \frac{1}{2}\left[\frac{dF_2}{dq_2} \pm \sqrt{(\frac{dF_2}{dq_2})^2 - 4(\frac{dF_2}{dq_1})^2}\right] \quad (36)$$

In the absence of any damping effects, if the above relation has two pure imaginary roots, the fixed point is a center point. On the other hand, if the solution includes two real eigenvalues with one positive and one negative root, it means that the fixed point is an unstable saddle point. Furthermore, in the presence of damping force, if the eigenvalues are non-real and of the form $\alpha \pm i\beta$, with $\alpha \neq 0$, then it is an unstable spiral point for $\alpha > 0$ and a stable spiral point for $\alpha < 0$.

3. Results

3.1. Validation

To check the soundness of present model the pull-in voltage of nano-scanner in the static case are determined and a comparison has been carried out with the reported results by Beni et al. [39]. To this end, the variation of pull-in angle versus the microstructure parameter (*l*/*t*) for some assigned values of applied voltage λ is presented in Fig. 2. According to this figure, one can see that excellent agreement with the reported results in the literature are obtained.

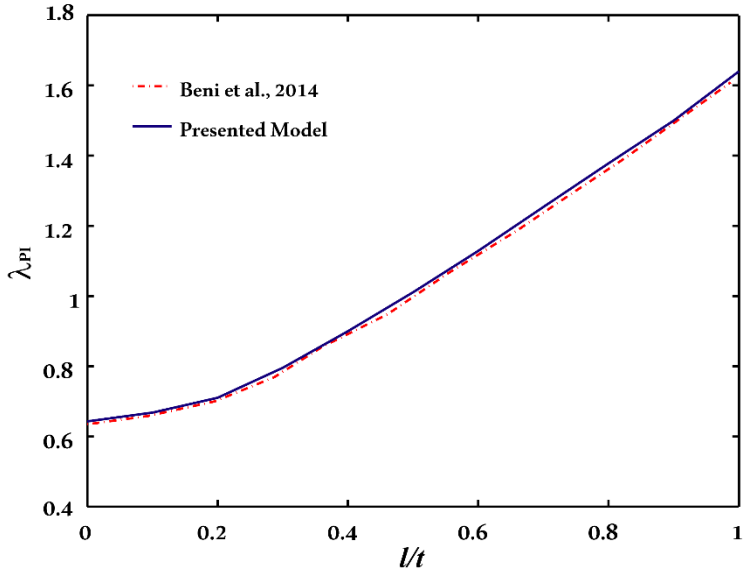

Fig. 2. Impact of microstructure parameter (l/t) on nondimentional pull-in voltage when (l_0=l_1=l_2=l)

In addition, the presented microstructure-dependent model is compared with experimental results in the literature [1]. Figure (3) compares the pull-in voltage predicted by the presented microstructure-dependent model with those obtained experimentally by Zhan et al. [1]. As seen while the classical model (l=0) can't predict the pull-in voltage accurately by considering l=300 nm the results of presented size dependent model are in very good agreement with those of experimental.

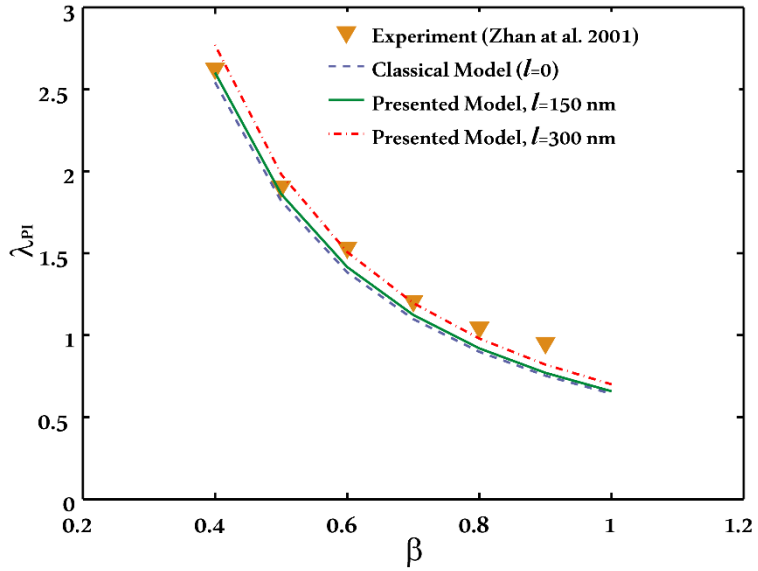

Figure 3. Comparison between the pull-in voltage of experimental measurement and those calculated by presented models (l_0=l_1=l_2=l)

3.2 Stability analysis

Figures 4 to 6 indicate the motion trajectories of the varactor with different actuation voltages. According to Fig. 4, in the absence of damping effects, there exist one stable center point and one unstable saddle node. In addition, there is a homoclinic orbit in the vicinity of saddle node. Homoclinic orbit originates from a saddle node via the unstable branch and returns to this node via the stable one. The homoclinic orbit separates the periodic region around the center point from the unstable region beyond the saddle node.

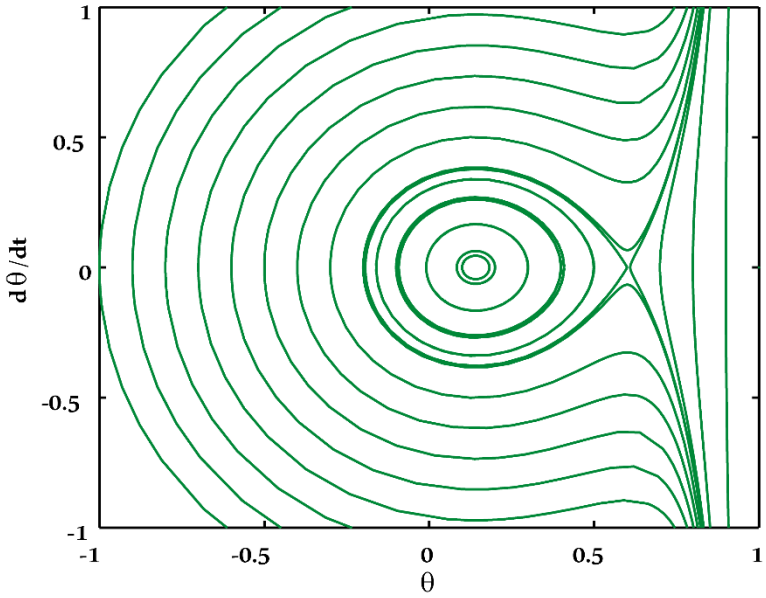

Fig. 4 Phase portrait in the absence of damping ($\eta = 0.2$, $\lambda < \lambda_{PI}$, $\alpha = 0.06$, $\beta = 0.84$)

The impact of damping parameter on the dynamic behavior of the varactor is shown in Fig. 5. The obtained results reveal that the stable center equilibrium point becomes a stable focus point if the damping parameter is taken into consideration. The varactor makes convergent oscillations near the focus point in the presence of the damping, and causes periodic oscillations if the damping is ignored. By increasing the applied voltage, the homoclinic orbit becomes smaller until the actuation voltage reaches the pull-in value. At this state, the trajectories diverge and the structure becomes unstable for any initial condition. As shown in figure 6, the homoclinic orbit disappears and the center and saddle points coalesce and replace by one saddle node.

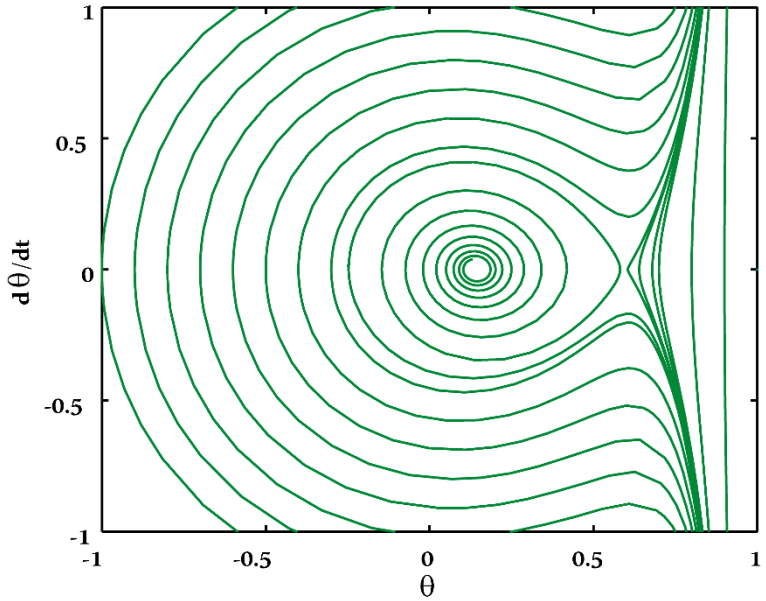

Fig. 5 Phase portrait in the presence of damping ($\eta = 0.2$, $\lambda < \lambda_{PI}$, $\alpha = 0.06$, $\beta = 0.84$)

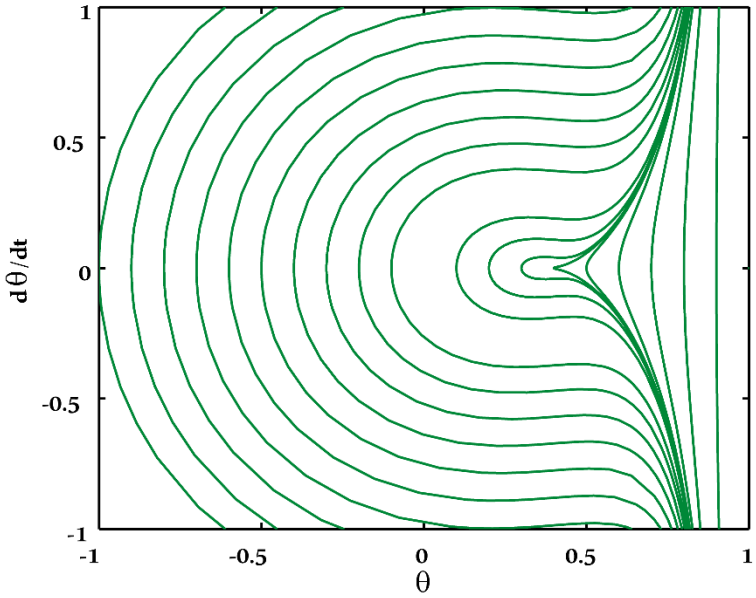

Fig. 6 Phase portrait for pull-in instability ($\eta = 0.2$, $\lambda = \lambda_{PI}$, $\alpha = 0.06$, $\beta = 0.84$)

3.3 Pull-in phenomenon

Figure 7 depicts the bifurcation diagrams where the applied voltage λ is plotted versus the equilibrium angles. In this figure, the equilibrium curves are plotted for some values of vdW force parameter. For micro-scale gaps ($\eta = 0$), if the actuation voltage is less than the pull-in value, there is one fixed point. For $\lambda > \lambda_{PI}$, the second fixed point appears in the phase plane. In this figure, the stable and unstable fixed-points are depicted by black and red colors, respectively. It should be noted that, the stable branch of equilibrium curves represents the center points and the unstable one denotes the existence of saddle nodes in the phase plane. Thereby, one can observe that in the absence of vdW attraction, for smaller values of applied voltage, the system undergoes periodic motions around the stable center point. On the other hand, by increasing λ , the second fixed point (saddle node) appears in the phase plane; beyond the unstable saddle node, the movable plate diverges to the ground. In addition, if the applied voltage approaches to the critical value, the equilibrium points merge and there exist no fixed points beyond this value (pull-in value). The corresponding tilt angle is called the "pull-in angle". Fig. 7, reveals that the maximum of the equilibrium curves decreases by increasing the vdW parameter. This means that vdW force decreases the pull-in angle (Θ_{PI}) and pull-in voltage (λ_{PI}) of the system.

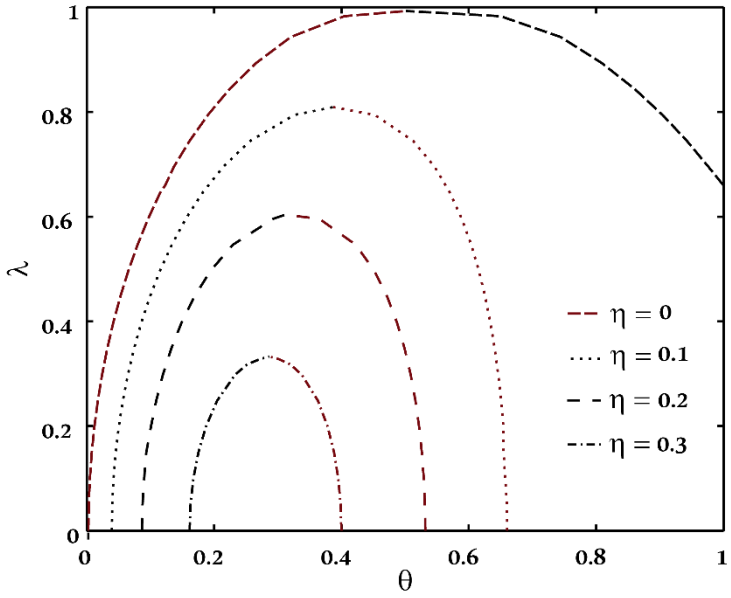

Fig.7. The position of equilibrium points versus the applied voltage for various vdW force

The impact of the applied voltage on the stability of the varactor is illustrated in Fig. 8. The non-dimensional frequency of vibrating varactor decreases by increasing λ. On the other hand, the pull-in phenomenon happens when the applied voltage reaches the critical values. Beyond the critical value, the torsional nano-varactor loses its stability and diverges to the rigid substrate.

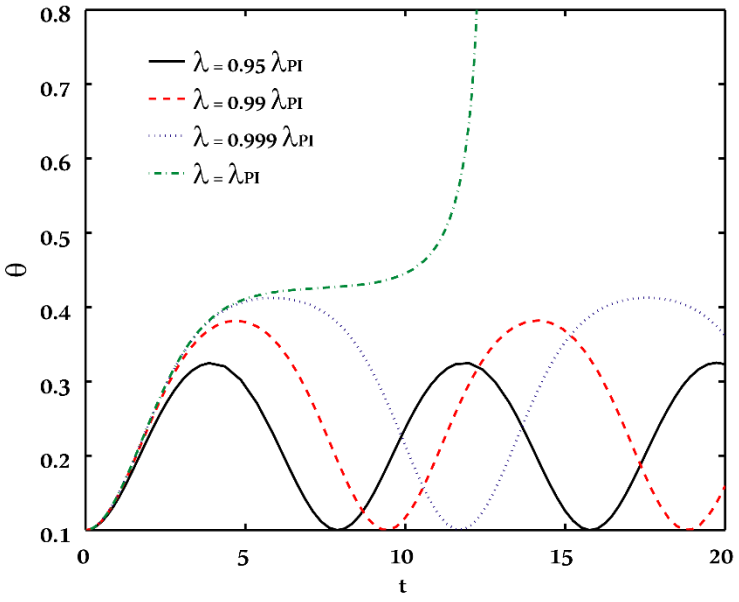

Fig. 8. Time history of the varactor: influence of the actuation voltage

3.4 Microstructure effect

Fig. 9 illustrates the position of equilibrium points versus the applied voltage for various values of the microstructure parameter J_C / J. As illustrated in Fig. 9 for $\lambda < \lambda_{PI}$ there exist two fixed points, however for $\lambda > \lambda_{PI}$ the system has no fixed point. This phenomenon shows saddle-node bifurcation in which unstable and stable branches coalesce at the same point in the state-control space. Furthermore, when the influence of microstructure is taken into account, the pull-in voltage

and pull-in angle of the nano-varactor will increase; in other words, the instability threshold of the system shifts upwards as the nano-structure shows the microstructure-dependent behavior

To examine the impact of vdW force on the stability of freestanding varactor ($\lambda = 0$), the equilibrium curves of the system plotted versus parameter η for different values of J_C / J . Figure 10 shows the position of the fixed points for free-standing nano-structure. By increasing the vdW attraction, two fixed-points become closer to each other and meet together at saddle node bifurcation. It means the saddle point bifurcation occurs at the critical tilt angle.

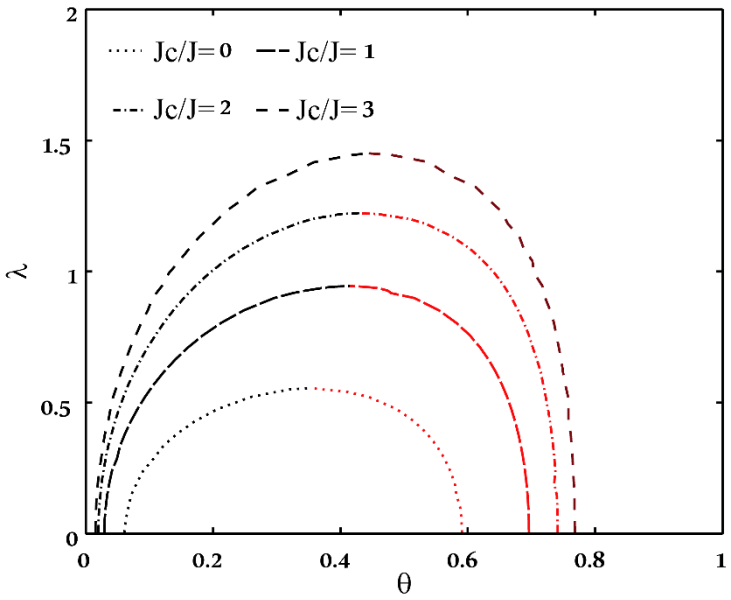

Fig. 9. The position of equilibrium points versus the applied voltage: the impact of microstructure

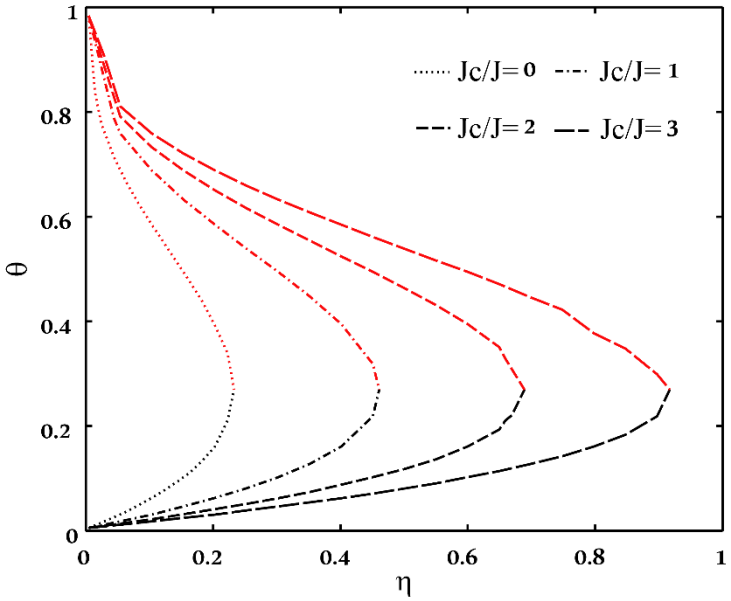

Fig. 10. The position of equilibrium points for freestanding actuator: the impact of microstructure

The time history of vibrating varactor for various values of microstructure parameter J_C / J at the corresponding dynamic pull-in points are illustrated in Fig. 11. When the actuation voltage parameter is considered as the control parameter. According to this figure, the pull-in time of the nano-varactor is decreased by increasing the microstructure parameter and the pull-in phenomenon occurs at higher

values of applied bias voltage. It is also concluded that as the value of microstructure parameter increases, the instability happens at higher Θ value.

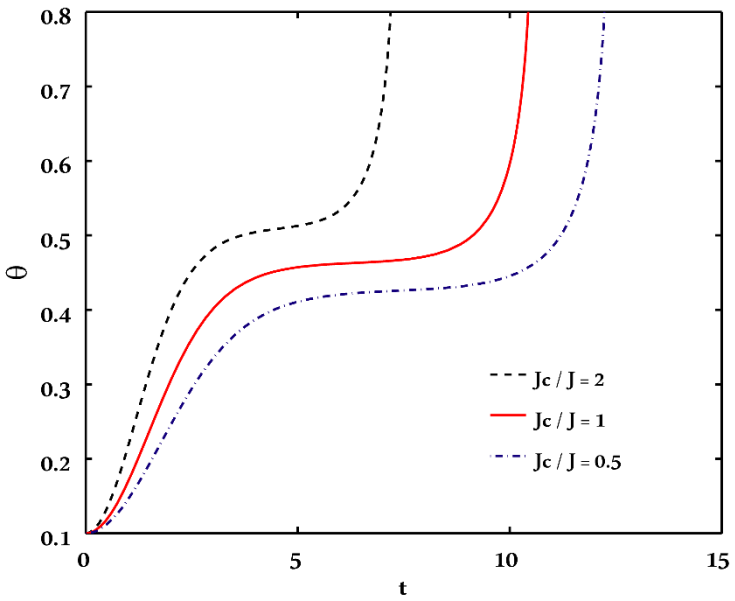

Fig. 11. Time histories for different values of microstructure parameter J_C / J at corresponding dynamic pull-in point considering the applied voltage as a control parameter

4 Conclusions

The microstructure-dependent dynamic behavior and instability analysis of a torsional varactor subject to electrostatic and vdW forces were studied. By employing the SGT, the governing equation of the varactor was derived. It was observed that the pull-in voltage increases by enhancing the microstructure parameter. On the other hand, increasing the microstructure effect increases the pull-in angle of the system. As the value of microstructure parameter increases, the pull-in time is decreased and instability happens at higher values of torsion angle. The system dynamics exhibits saddle-node bifurcation in which unstable and stable branches coalesce at the corresponding pull-in voltage. The stable center point becomes a stable focus point as the damping parameter is taken into consideration.

Appendix

Using Saint-Venant's approach and substituting equation (11) in (2)-(5) the component of strain tensor can be determined as

$$\varepsilon_{11}=\varepsilon_{22}=\varepsilon_{33}=\varepsilon_{12}=0,\quad \varepsilon_{31}=\varepsilon_{31}=\frac{1}{2}\Omega\left(\frac{\partial\psi}{\partial X}-Y\right),$$

$$\varepsilon_{32}=\varepsilon_{23}=\frac{1}{2}\Omega\left(\frac{\partial\psi}{\partial Y}+X\right),\quad \gamma_1=\gamma_2=\gamma_3=0,$$

$$\eta^{(1)}_{333}=-\frac{1}{5}\Omega\nabla^2\psi,\qquad \eta^{(1)}_{111}=\eta^{(1)}_{222}=0,$$

$$\eta^{(1)}_{312}=\eta^{(1)}_{123}=\eta^{(1)}_{231}=\eta^{(1)}_{213}=\eta^{(1)}_{132}=\eta^{(1)}_{321}=\frac{1}{3}\Omega\frac{\partial^2\psi}{\partial X\,\partial Y},$$

$$\eta^{(1)}_{322}=\eta^{(1)}_{232}=\eta^{(1)}_{112}=\frac{1}{15}\Omega\left(4\frac{\partial^2\psi}{\partial Y^2}-\frac{\partial^2\psi}{\partial X^2}\right),\tag{A1}$$

$$\eta^{(1)}_{311}=\eta^{(1)}_{131}=\eta^{(1)}_{113}=\frac{1}{15}\Omega\left(4\frac{\partial^2\psi}{\partial X^2}-\frac{\partial^2\psi}{\partial Y^2}\right),$$

$$\chi^s_{33}=\Omega,\ \chi^s_{11}=\frac{\Omega}{2}\left(\frac{\partial\psi}{\partial X\,\partial Y}-1\right),\qquad \chi^s_{22}=-\frac{\Omega}{2}\left(\frac{\partial\psi}{\partial X\,\partial Y}+1\right),$$

$$\chi^s_{12}=\chi^s_{21}=\frac{\Omega}{4}\left(\frac{\partial^2\psi}{\partial Y^2}-\frac{\partial^2\psi}{\partial X^2}\right)$$

By substituting equations (A1) in (6)-(9), the stress components are obtained as

$$\sigma_{13}=\sigma_{31}=\frac{1}{2}\Omega\left(\frac{\partial\psi}{\partial X}-Y\right),\qquad \sigma_{23}=\sigma_{32}=\frac{1}{2}\Omega\left(\frac{\partial\psi}{\partial Y}+X\right),$$

$$\tau^{(1)}_{333}=-\frac{2}{5}\mu l_1^2\,\Omega\nabla^2\psi,$$

$$\tau^{(1)}_{311}=\tau^{(1)}_{131}=\tau^{(1)}_{113}=\frac{2}{15}\mu l_1^2\,\Omega\left(4\frac{\partial^2\psi}{\partial X^2}-\frac{\partial^2\psi}{\partial Y^2}\right),$$

$$\tau^{(1)}_{322}=\tau^{(1)}_{232}=\tau^{(1)}_{112}=\frac{2}{15}\mu l_1^2\,\Omega\left(4\frac{\partial^2\psi}{\partial Y^2}-\frac{\partial^2\psi}{\partial X^2}\right),$$

$$\tau^{(1)}_{312}=\tau^{(1)}_{123}=\tau^{(1)}_{231}=\tau^{(1)}_{213}=\tau^{(1)}_{132}=\tau^{(1)}_{321}=\frac{2}{3}\mu l_1^2\,\Omega\frac{\partial^2\psi}{\partial X\,\partial Y},\tag{A2}$$

$$m^s_{33}=2\,\mu l_2^2\,\Omega,\ \chi^s_{11}=\mu l_2^2\,\Omega\left(\frac{\partial^2\psi}{\partial X\,\partial Y}-1\right),$$

$$m^s_{22}=-\mu l_2^2\,\Omega\left(\frac{\partial^2\psi}{\partial X\,\partial Y}+1\right),$$

$$m^s_{12}=m^s_{21}=\mu l_2^2\,\frac{\Omega}{2}\left(\frac{\partial^2\psi}{\partial Y^2}-\frac{\partial^2\psi}{\partial X^2}\right)\quad m^s_{11}=2\,\mu\Omega l_2^2$$

The equilibrium equation is in the axial direction is written as [32]:

$$\sigma_{23,3}+\sigma_{21,1}-\frac{1}{2}\left(m^s_{33}-m^s_{11}\right)_{,31}$$
$$+\frac{1}{2}m^s_{31,33}-\frac{1}{2}m^s_{31,11}-\tau^{(1)}_{233,33}-\tau^{(1)}_{211,11}-2\,\tau^{(1)}_{231,31}=0\tag{A3}$$

By substituting relations (A1) and (A2) into equations (A3) and after some elaboration, the governing equation of the system can be obtained as:

$$\nabla^2\left[\psi-\left(\frac{8l_1^2}{15}+\frac{l_2^2}{4}\right)\nabla^2\psi\right]=0 \tag{A4}$$

The boundary conditions of the torsion beam are [32]:

$$\frac{\partial\psi}{\partial n}-\left(\frac{8l_1^2}{15}+\frac{l_2^2}{4}\right)\nabla^2\left(\frac{\partial\psi}{\partial n}\right)-\left(\frac{2l_1^2}{3}+\frac{l_2^2}{2}\right)\left(\frac{\partial^2\psi}{\partial n\partial t}\right)=Yn_X-Xn_Y$$

$$\left(\frac{8l_1^2}{15}+\frac{l_2^2}{4}\right)\nabla^2\psi-\left(\frac{2l_1^2}{3}+\frac{l_2^2}{2}\right)\left(\frac{\partial^2\psi}{\partial t^2}\right)=0$$

$$\frac{1}{2\mu}\left(\frac{\partial\psi}{\partial X}-Y\right)+\frac{l_2^2}{4}\left(\frac{\partial^3\psi}{\partial X^3}+\frac{\partial^2\psi}{\partial X\,\partial Y^2}\right)+\frac{16l_1^2}{15}\left(\frac{\partial^3\psi}{\partial X^3}+\frac{\partial^3\psi}{\partial X\,\partial Y^2}\right)=\frac{\partial\psi}{\partial X}-Y-\left(\frac{16l_1^2}{15}-\frac{l_2^2}{4}\right)^2\nabla^2\left(\frac{\partial\psi}{\partial X}\right. \tag{A5}$$

$$\frac{1}{2\mu}\left(\frac{\partial\psi}{\partial Y}+X\right)+\frac{l_2^2}{4}\left(\frac{\partial^3\psi}{\partial Y^3}+3\frac{\partial^3\psi}{\partial Y\,\partial X^2}\right)-\frac{16l_1^2}{15}\left(\frac{\partial^3\psi}{\partial Y^3}+\frac{\partial^3\psi}{\partial X^2\partial Y}\right)=\frac{\partial\psi}{\partial Y}+X-\left(\frac{16l_1^2}{15}-\frac{l_2^2}{4}\right)^2\nabla^2\left(\right.$$

where n and t are normal and tangential direction of lateral surface of the beam. By solving the equations via series solution, ψ are determined (see ref. [32]).

References

[1] Zhang, X. M., Chau, F. S., Quan, C., Lam, Y. L., & Liu, A. Q. (2001). A study of the static characteristics of a torsional micromirror. Sensors and Actuators A: Physical, 90(1), 73-81.

[2] Lin, W. H., & Zhao, Y. P. (2007). Stability and bifurcation behaviour of electrostatic torsional NEMS varactor influenced by dispersion forces. Journal of Physics D: Applied Physics, 40(6), 1649.

[3] Beni, Y. T. (2015). Using Modified Couple Stress Theory to Investigate the Size-Dependent Instability of Rotational Nano-Actuator under Van der Waals Force. Academic Platform Journal of Engineering and Science, 3(1), 42-47.

[4] Taghizadeh, M., & Mobki, H. (2014). Bifurcation analysis of torsional micromirror actuated by electrostatic forces. Archives of Mechanics, 66(2), 95-1111.

[5] Venkatesh, C., Bhat, N., Vinoy, K. J., & Grandhi, S. (2012). Microelectromechanical torsional varactors with low parasitic capacitances and high dynamic range. Journal of Micro/Nanolithography, MEMS, and MOEMS, 11(1), 013006-1.

[6] Moeenfard, H., Darvishian, A., & Ahmaidan, M. T. (2013). A coupled bending-torsion model for electrostatically actuated torsional nano/micro-actuators with considering influence of van der Waals force. Acta Mechanica, 224(8), 1791–1800.

[7] Degani, O., & Nemirovsky, Y. (2002). Design considerations of rectangular electrostatic torsion actuators based on new analytical pull-in expressions. Journal of Microelectromechanical Systems, 11(1), 20-26.

[8] Malihi, S., Beni, Y. T., & Golestanian, H. (2016). Analytical modeling of dynamic pull-in instability behavior of torsional nano/micromirrors under the effect of Casimir force. Optik - International Journal for Light and Electron Optics, 127(10), 4426–4437.

[9] Guo, J. G., & Zhao, Y. P. (2004). Influence of van der Waals and Casimir forces on electrostatic torsional actuators. Microelectromechanical Systems, Journal of, 13(6), 1027-1035.

[10] Guo, J. G., & Zhao, Y. P. (2006). Dynamic stability of electrostatic torsional actuators with van der Waals effect. International Journal of Solids and Structures, 43(3), 675-685.

[11] Moeenfard, H., Darvishian, A., & Ahmaidan, M. T. (2012). Static behavior of nano/micromirrors under the effect of Casimir force, an analytical approach. Journal of Mechanical Science and Technology, 26(2), 537–543.
[12] Sedighi, H. M., & Shirazi, K. H. (2015). Dynamic pull-in instability of double-sided actuated nano-torsional switches. Acta Mechanica Solida Sinica, 28(1), 91-101.
[13] Chen, H., Sun, W.J., Sun, Z.D., Yeow, J.T.W. (2013). Second-order sliding mode control of a 2D torsional MEMS micromirror with sidewall electrodes. Journal of Micromechanics and Microengineering, 23, 015006.
[14] Taghizadeh, M., & Mobki, H. (2014). Bifurcation analysis of torsional micromirror actuated by electrostatic forces. Archives of Mechanics, 66(2), 95-111.
[15] Zhang, W. M., Yan, H., Peng, Z. K.,& Meng G. (2014). Electrostatic pull-in instability in MEMS/NEMS: A review. Sensors and Actuators A, 214, 187–218
[16] Wen-Hui, L., & Ya-Pu, Z. (2003). Dynamic behaviour of nanoscale electrostatic actuators. Chinese Physics Letters, 20(11), 2070.
[17] Xiang, W., & Lee, C. (2010). Nanoelectromechanical torsion switch of low operation voltage for nonvolatile memory application. Applied Physics Letters, 96(19), 193113.
[18] Sedighi, H. M., & Shirazi, K. H. (2015). Dynamic pull-in instability of double-sided actuated nano-torsional switches. Acta Mechanica Solida Sinica, 28(1), 91-101.
[19] Guo, J. G., Zhou, L. J., & Zhao, Y. P. (2009). Instability analysis of torsional MEMS/NEMS actuators under capillary force. Journal of Colloid and Interface Science, 331(2), 458-462.
[20] Shabani, R., Tariverdilo, S., Rezazadeh, G., & Agdam, A. P. (2011). Nonlinear vibrations and chaos in electrostatic torsional actuators. Nonlinear Analysis: Real World Applications, 12(6), 3572-3584.
[21] Xiao, Z., Wu, X., Peng, W., & Farmer, K. R. (2001). An angle-based design approach for rectangular electrostatic torsion actuators. Microelectromechanical Systems, Journal of, 10(4), 561-568.
[22] Younse, J. M. (1993). Mirrors on a chip. Spectrum, IEEE, 30(11), 27-31.
[23] Abdi, J., Koochi, A., Kazemi, A. S., & Abadyan, M. (2011). Modeling the effects of size dependence and dispersion forces on the pull-in instability of electrostatic cantilever NEMS using modified couple stress theory. Smart Materials and Structures, 20(5), 055011.
[24] Yang, F. A. C. M., Chong, A. C. M., Lam, D. C. C., & Tong, P. (2002). Couple stress based strain gradient theory for elasticity. International Journal of Solids and Structures, 39(10), 2731-2743.
[25] Lam, D. C. C., Yang, F., Chong, A. C. M., Wang, J., & Tong, P. (2003). Experiments and theory in strain gradient elasticity. Journal of the Mechanics and Physics of Solids, 51(8), 1477-1508.
[26] Batra, R. C., Porfiri, M., & Spinello, D. (2008). Effects of van der Waals force and thermal stresses on pull-in instability of clamped rectangular microplates. Sensors, 8(2), 1048-1069.
[27] Farrokhabadi, A., Rach, R., & Abadyan, M. (2013). Modeling the static response and pull-in instability of CNT nanotweezers under the Coulomb and van der Waals attractions. Physica E: Low-dimensional Systems and Nanostructures, 53, 137–145.
[28] Ramezani, A., Alasty, A., & Akbari, J. (2007). Closed-form solutions of the pull-in instability in nano-cantilevers under electrostatic and intermolecular surface forces. International Journal of Solids and Structures, 44(14), 4925-4941.
[29] Soroush, R., Koochi, A., Kazemi, A. S., Noghrehabadi, A., Haddadpour, H., & Abadyan, M. (2010). Investigating the effect of Casimir and van der Waals attractions on the electrostatic pull-in instability of nano-actuators. Physica scripta, 82(4), 045801.
[30] Lin, W. H., & Zhao, Y. P. (2007). Stability and bifurcation behaviour of electrostatic torsional NEMS varactor influenced by dispersion forces. Journal of Physics D: Applied Physics, 40(6), 1649.

[31] Sedighi, H. M. (2014). The influence of small scale on the pull-in behavior of nonlocal nanobridges considering surface effect, Casimir and Van der Waals attractions. International Journal of Applied Mechanics, 6(3), 1450030

[32] Tong, P., Yang, F., Lam, D. C., & Wang, J. (2004, March). Size effects of hair-sized structures–torsion. In Key Engineering Materials (Vol. 261, pp. 11-22).

[33] Tsiatas, G. C., & Katsikadelis, J. T. (2011). A new microstructure-dependent Saint–Venant torsion model based on a modified couple stress theory. European Journal of Mechanics-A/Solids, 30(5), 741-747.

[34] Huang, J. M., Liu, A. Q., Deng, Z. L., Zhang, Q. X., Ahn, J., & Asundi, A. (2004). An approach to the coupling effect between torsion and bending for electrostatic torsional micromirrors. Sensors and Actuators A: Physical, 115(1), 159-167.

[35] Beni, Y. T., Koochi, A., Kazemi, A. S., & Abadyan, M. (2012). Modeling the influence of surface effect and molecular force on pull-in voltage of rotational nano–micro mirror using 2-DOF model. Canadian Journal of Physics, 90(10), 963-974.

[36] Sattler, R., Plötz, F., Fattinger, G., & Wachutka, G. (2002). Modeling of an electrostatic torsional actuator: demonstrated with an RF MEMS switch. Sensors and Actuators A: Physical, 97, 337-346.

[37] Ouakad, H. M., & Younis, M. I. (2011). Natural frequencies and mode shapes of initially curved carbon nanotube resonators under electric excitation. Journal of Sound and Vibration, 330(13), 3182-3195.

[38] Ouakad, H. M., & Younis, M. I. (2010). Nonlinear dynamics of electrically actuated carbon nanotube resonators. Journal of Computational and Nonlinear Dynamics, 5(1), 011009.

[39] Beni, Y. T., Koochi, A., & Abadyan, M. (2014). Using modified couple stress theory for modeling the size-dependent pull-in instability of torsional nano-mirror under Casimir force. International Journal of Optomechatronics, 8(1), 47-71.